



ORIGINAL ARTICLE

Multimode Grasping Soft Gripper Achieved by Layer Jamming Structure and Tendon-Driven Mechanism

AU1 ▶ Bin Fang,^{1,*} Fuchun Sun,¹ Linyuan Wu,² Fukang Liu,¹ Xiangxiang Wang,³ Haiming Huang,² Wenbing Huang,¹ Huaping Liu,¹ and Li Wen^{4,†}

Abstract

Robotic grasping has become increasingly important in many application areas such as industrial manufacturing and logistics. Because of the diversity and uncertainty of objects and environments, common grippers with one single grasping mode face difficulties to fulfill all the tasks. Hence, we proposed a soft gripper with multiple grasping modes in this study. The gripper consists of four modular soft fingers integrated with layer jamming structure and tendon-driven mechanism. Each finger's rotating shaft of the base uses a torsional spring to decouple the bending deformation and relative rotation. An octopus-mimicking vacuum sucker is installed in the fingertip to generate suction. The effectiveness of the bending deformation and variable stiffness of the design were proved by finite element simulation. Thus, the control model of the finger was built, and the control strategy of multimode grasping of the gripper was proposed. Three control modes were designed to realize the four anthropomorphic grasping modes, including wrap, pinch, hook, and suck. Furthermore, the grasping performance was evaluated to show the abilities. The experiments indicated the superior performance of the proposed gripper and the multimode grasping ability that satisfies various grasping tasks.

AU4 ▶ Keywords: multimode grasping, tendon-driven, layer jamming

Introduction

AU5 ▶ IN RECENT YEARS, soft robotics have increasingly drawn the attention of researchers and engineers.^{1,2} Soft materials, such as silicone, are the main components of soft robots and provide bioinspired designs and infinite degrees of freedom for robots.³ These features allow soft robots to easily achieve adaptation without complex control schemes.⁴ For example, the compliance of soft robotic grippers (SRGs) allows the grippers to overcome the challenge of grasping objects with different fragility, size, hardness, and geometry. Therefore, SRGs have huge potential in universal grasping compared with traditional rigid grippers.^{5–7}

In general, SRGs have three typical driving mechanisms,⁸ including fluidic actuation,⁹ actuation based on the deforma-

tion of smart materials,¹⁰ and the tendon-driven mechanism.^{11,12} Fluidic actuation includes pneumatic-driven and hydraulic-driven mechanisms.^{13,14} Hydraulic-driven grippers are powerful and fast. However, it is difficult to simultaneously achieve a high liquid pressure output and a lightweight fluidic device, and the contradiction between the response speed and large deformation of soft actuators also restricts the fluidic actuation method.¹⁵ Smart materials such as dielectric elastomers,¹⁶ electroactive polymers,¹⁷ and shape memory alloys (SMAs)¹⁸ can also be deployed to actuate soft grippers. However, they rely on external physical conditions that affect their strength, stability, and accuracy. The tendon-driven mechanism¹⁹ is a traditional method that exhibits superior performance in terms of speed and precision. It depends on the position-driven motor and transmission mechanism.

AU2 ▶ ¹Tsinghua National Laboratory for Information Science and Technology, Department of Computer Science and Technology, Tsinghua University, Beijing, China.

AU3 ▶ ²School of Electronics and Information Engineering, Shenzhen University, Shenzhen, China.

³Institute of Mechanical Engineering, Anhui University of Technology, Ma'anshan, Anhui, China.

⁴School of Mechanical Engineering and Automation, Beihang University, Beijing, China.

*ORCID ID (<https://orcid.org/0000-0002-9149-7336>).

†ORCID ID (<https://orcid.org/0000-0002-1498-3103>).

SRG materials improve the flexibility and interaction safety of SRGs but weaken the load capacity because of a lack of stiffness and strength. Thus, several methods to improve the stiffness of SRGs have been proposed.^{20,21} Electrorheological (ER)²² and magnetorheological (MR) fluids²³ require additional drivers to produce high voltages (in ER) or magnetic power (in MR) to realize state switching from soft to stiff. Low melting point materials (LMPMs)²⁴ embedded within a heating element can achieve a wide range of stiffness variations. Shape memory materials mainly include SMAs and shape memory polymers (SMPs).^{25,26} However, the response speed of LMPMs and SMPs are extremely slow, and the heating process is difficult to control. SMAs also require an external heating device and have limited stiffness variation ratios. Similarly, conductive polylactic acid²⁷ exhibits a superior performance in variable stiffness but the phase transition is slow. Unlike layer jamming structures (LJSs) with layer materials in chambers,^{28,29} granular jamming structures consist of a flexible sealed chamber, which contains particle materials and occupies more space than the layer ones for the same stiffness improvement.³⁰ The fiber jamming structure is the fiber material, such as long fiber-reinforced plastics³¹ and square cross-sectioned fibers,³² sealed in a jamming cavity. These types of fiber jamming structures enable tunable bending stiffness in multiple directions, but need a three-dimensional structure for getting enough variable stiffness ratio. Some vacuum jamming structures depend on the air pressure difference between the outside and inside of a granular, layer, or fiber jamming cavity for variable stiffness,³²⁻³⁴ with considerable advantages in response speed and considerable significance in real-world applications. Several layer materials can be used for this purpose, such as paper, PET, sandpaper, and polyimide.^{33,35,36} Test results³⁵ on the thickness, weight, and variable stiffness range performance of some layer materials provide a selection reference for other researchers. After test-

ing and comparing, we found that the paper layer is easily accessible, lightweight, easy to modify and cut, and sufficiently soft but inelastic. Some previous works^{29,37} also proved that paper is an effective layer material.

Two layer jamming grippers have been proposed in the state-of-the-art and exhibited excellent stiffness improvement effects,^{29,38} but just like the most grippers, the above two grippers have only one single grasping mode. It is difficult to fulfill all the tasks because of the diversity and complexity of the objects and environment. The soft gripper proposed by Wang *et al.*³⁹ owns two grasping modes but it needs manual switch operation. The soft gripper and hand proposed in Zhong *et al.*⁴⁰ and Deimel and Brock,⁹ respectively, are featured by grasping modes (except sucking) that require the finger rolling up so that the grasping modes cannot grasp special objects like flat objects. The proposed gripper is developed with multiple grasping modes, including enveloping grasping, clamping, sucking, and hooking. Effective variable stiffness improves the multimode grasping. The combination of the vacuum operation and tendon-driven methods enables the development of multimode grasping. In similar examples, grippers with suckers^{41,42} own sucking and grasping skills at the same time. The proposed gripper developed the four effective modes listed above and was designed by integrating a controlling vacuum and tendon device to realize various grasping modes corresponding to objects of various sizes, shapes, and weights. To intensify the tendon-driven capacity, converging tendon routing⁴³ was applied to strengthen the tip resistance ability.

Design and Manufacture

Design

The structure of the proposed SRG is shown in Figure 1A. It consists of four soft fingers that can provide more grasping

AU6 ▶

◀ F1

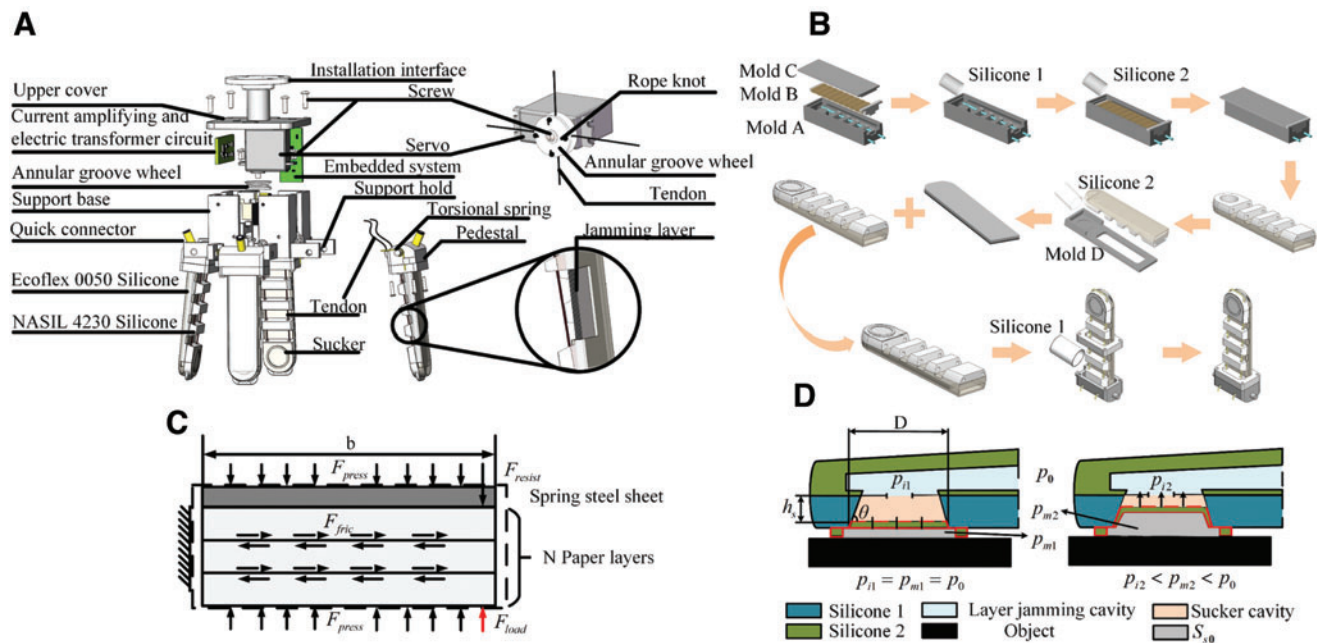


FIG. 1. Model of the gripper. (A) Holistic structure of the proposed gripper with an explosion diagram. (B) Fabrication process diagram of the finger. (C) Variable stiffness principle analysis diagram. (D) Schematic diagram of the sucker on the fingertip. Color images are available online.

abilities than two or three fingers. The fingers include a soft chamber, jamming layers, and a 3D-printed pedestal. The soft chamber is manufactured using two types of silicone with a tendon path and a sucker. Layer materials are inserted into the soft chamber of the LJS, and the chamber is buckled into a pedestal fastened to a quick air connector. The finger integrates the variable stiffness performance and tendon drive structure. The tendon structure, servo, valve, and control circuits are mounted on a base. An annular groove wheel is tightly buckled on the servo's output axis, and four through holds are evenly distributed around the side of the groove wheel. The servo drives the groove wheel to drag the tendon for deformation of the fingers and rotation of the pedestal. The servo and valve are fixed on the inside of the base with an embedded system. Moreover, a torsional spring is fixed to the left cylindrical axle on the pedestal. It can decouple the relative rotation and bending deformation. Before vacuuming, the torsional spring restricts the pedestal and transmits a major pulling force to induce bending of the soft finger. After vacuuming, the stiffness enhancement of the soft finger limits the bending deformation, and when the pulling force overpasses the torque force of the torsional spring, the extra part of pulling force is transmitted to rotate the pedestal. The torsional spring enables the multimode grasping.

Variable stiffness principle. Variable stiffness is effective to compensate the lack of stiffness. In this study, layer jamming is adopted to adjust the stiffness. Several independent layers are present inside the soft chamber. The layer material includes paper layers and a spring steel sheet. As the side section view in Figure 1C, paper layers are cut to the same size and neatly stacked together, with the spring steel sheet being aligned and placed on the top surface of the paper layers. During the operation, the vacuum device extracts the air in a sealed chamber such that the layers are firmly bonded together and the finger becomes stiff. The friction force between the paper layers is the source of the force that resists deformation. As shown in Figure 1C, a critical state exists when a maximum external load force, which is equal to the sum effect of all the friction forces between the two layers, and the resistance force of the spring steel sheet is applied to the end point of the vacuumed LJS. Furthermore, when the finger is in the vertical state, the spring steel sheet resists deformation under an external force. When the finger is in bending state, the spring steel sheet becomes resilient for reconstruction. Based on the above analysis, the relationship between the maximum bearing capacity $F_{\max\text{load}}$ and LJS parameters can be characterized intuitively as follows:

$$F_{\max\text{load}} = \begin{cases} N \cdot \mu \cdot A_{xz} \cdot p_{\text{vacuum}} + F_{\text{resist}} & (\text{vertical}) \\ N \cdot \mu \cdot A_{xz} \cdot p_{\text{vacuum}} - F_{\text{resist}} & (\text{bending}) \end{cases} \quad (1)$$

where N is the number of layers, p_{vacuum} is the pressure difference between the inner chamber and atmospheric pressure, A_{xz} is the contact area of the layers, μ is the friction coefficient of the layers, and F_{resist} is the force from the spring steel sheet resisting or recovering the deformation.

In Eq. (1), when the finger is in a vertical state, F_{resist} is the resisting force for deformation. When the finger is in bending state, F_{resist} acts as a recovering force for deformation. Moreover, $F_{\max\text{load}}$ has a limitation such that an overlarge external force still produces bending deformation. Equation (1) shows that the stiffness of the LJS is affected by the number of layers, bending force from pressure difference, size of the contact area, and surface friction force of each layer. Therefore, an appropriate layer size, number of layers, and adequate friction force factor of the layer material should be considered in the design and production.

Principle of the sucker's design. To furtherly increase grasping stability and diversity, a sucker was designed in the fingertip. The inner cavity of the sucker is connected to the jamming structure such that they work synchronously. A thin gap between the sucker's edge and the object's surface is unavoidable, which generates the escape of air and weakens the stiffness performance. Thus, the sucker was designed into a two-stage air cavity structure. A thin film covers the surface of the sucker cavity, as shown in Figure 1D. When vacuuming, the air pressure p_{i1} in the sucker cavity is vacuumed into p_{i2} such that the pressure difference of p and p_{m1} pressurizes the film to cover the inner wall of the sucker. Deformation of the film enlarges the closed space S_{s0} between the sucker and objects, making the initial air pressure p_{m1} in S_{s0} , which is equal to the ambient atmospheric pressure, decrease to p_{m2} at the same time. Furthermore, the air pressure difference Δp of p_{m2} and atmospheric pressure p_0 generates the adsorption force to catch objects.

The principle of the sucker is described as the ideal gas equilibrium,

$$pV = nRT \quad (2)$$

where p , V , and n represent the pressure, volume, and amount of the ideal gas, respectively, and T is the temperature of the gas. R is a constant equal to $8.31 \text{ J}/(\text{mol} \cdot \text{K})$.

For the sucker, T is invariable and n is constant; thus, an increase in V results in a decrease in p . The volume variation ΔV of S_{s0} is calculated as follows:

$$\Delta V = V_2 - V_1 \quad (3)$$

where V_1 and V_2 are the initial and the latest volume values of S_{s0} , respectively. Moreover, the sucker cavity is a circular truncated cone, and the deformation process of S_{s0} is reduced to the volume increase of the circular truncated cone:

$$\begin{aligned} \Delta V &= \left\{ \frac{1}{3} \pi \left[D^2 + (D - \Delta h_s \cot(\theta))^2 + D(D - \Delta h_s \cot(\theta)) \right] \Delta h_s + V_1 \right\} - V_1 \\ &= \frac{1}{3} \pi \left[D^2 + (D - \Delta h_s \cot(\theta))^2 + D(D - \Delta h_s \cot(\theta)) \right] \Delta h_s \\ &= \frac{1}{3} \pi \left[3D^2 - 3D\Delta h_s \cot(\theta) + (\Delta h_s \cot(\theta))^2 \right] \Delta h_s \end{aligned} \quad (4)$$

where D is the diameter of the sucker's bigger circle, θ is the angle of inclination of the inner wall, and Δh_s is the height variation value of S_{s0} .

Based on the above analysis, the adsorption force formula is as follows:

$$F_{abs} = \Delta p S = \frac{\Delta V}{\Delta V + V_1} p_{m1} S \quad (5)$$

where S is the contact area of the sucker with objects. Hence the adsorption force of the sucker is related to the volume variation and contact area. A larger volume variation and larger contact area can lead to higher adsorption capacity.

Principle of finger converging Tendon design. Referring to the study,⁴³ converging tendon design for fingers has the advantage of increasing the stiffness of the soft fingertip. The slope of the converging routing is $a = -b/L$, where b is the initial radius at the soft finger base and L is the effective length of the finger.

When parameter a is set as $-1/6$, the convergent finger can show significantly higher resistance to tip loads compared with the parallel tendon design finger. However, considering the limitations of the LJS's size and the sucker structure, the parameter a is halved as $-1/12$ (where L and b are 108 and 18 mm, respectively), and the tip loading capacity is between those of the parallel tendon design and the best converging design. Moreover, a U -shaped tendon is installed instead of a single line at the neutral axis centerline, mainly to make it easier to pull the soft fingers.

Manufacturing process

Figure 1B shows the fabrication process for the finger with the LJS and sucker. Four parts of molds are used and filled with liquid silicone: a main base (mold A), a center rectangular core (mold B), a top cap (mold C), and a bottom base for the covering membrane on the fingertip (mold D), and all are manufactured with a 3D printer.

In the first step, two aluminum bars are infixed into mold A to shape the tendon path. Then, liquid silicone 1 (NASIL 4230; Nabue New Material, Inc.) is poured into the groove of mold A. Silicone 1, with a hardness shore of 28 A, is solidified from liquid silicone 1 and has adequate resistance to bear the tendon force across the path. After curing of liquid silicone 1, mold B, with a piece of nylon fiber packing around it, is buttoned into mold A, and another softer liquid silicone 2 (Ecoflex 0050; Smooth-On, Inc.), whose solidified silicone hardness is 50 (shore 00), is poured into this assembling. With mold C covering, the molds are put into an oven to cure, and a silicone chamber with two types of silicone material is fabricated. Mold D is the foundation base with an annular concave structure, which is designed to produce the sucker surface. After liquid silicone 1 fills in the concave structure, the solidified silicone chamber above is placed on mold D, and then it is put into the oven again. After the third curing process, a thin silicone film covers the tip surface of the finger, and an intact soft chamber is finished.

In the second step, print papers are cut into many sheets (24×110 mm). In addition, thin hot-melt adhesive films are fully coated on one side of print paper surface A to improve the friction coefficient. The stickiness of the hot-melt adhesive film almost disappears after cooling; thus, the use of

adhesive film does not limit the relative movement of the print paper sheets. Surface A has 18 pieces of paper sheets, which are stacked together layer by layer neatly but loosely. The spring steel sheet, which is tailored to the same size as the paper sheet, is placed on the stacked paper layers. Next, the spring sheet and paper sheets are stuffed into the layer jamming cavity.

In the last step, a tendon is passed through the tendon path on the soft chamber in a U -shape. The pedestal has two cylindrical axles on two sides to bear the weight of the finger and simultaneously provide a rotation function. The soft chamber is pushed into the pedestal, and the tendon holds at the bottom of the pedestal. Liquid silicone 1 is poured into the pedestal inner cavity and cured with the soft chamber, integrating the soft chamber and pedestal together. Then, a rectangular fixed collar locks the soft chamber with four screws on the pedestal. Finally, a quick connector is screwed down into the pedestal air channel, which is convenient for installation or dismounting.

Regarding the above steps, mold B is wrapped with a piece of nylon fabric before being inserted into mold A. The nylon fabric, which sufficiently infiltrates and integrates with the liquid silicone, is used to reinforce the circumferential and axial constraints. The flexible and inelastic nylon fabric, which is integrated with the soft chamber, prevents stretch deformation of the soft chamber. Hence, the chamber wall can keep the jamming layers relatively static and tight after vacuum operation. The nylon also impedes the slide between the layers and strengthens the stiffness change effect.

The paper sheets in the layer jamming cavity are axially soft but radially coriaceous, indicating that they are easy to bend but hard to tear. Moreover, the spring steel with a thickness of ~ 0.1 mm is stiff in the axial direction but elastic in the radial direction and, thus, can return to the original form after withdrawal of an external force. The performance of the spring steel sheet helps the finger to quickly recover to the upright state without external power, which simplifies the transmission mechanism and also reduces energy consumption. Moreover, because the paper is too flexible to bear the twist that is the unrecoverable deformation when excessive force is applied, it is necessary to ensure that the twist resist ability surpasses the friction force between the layers. The addition of the spring steel sheet can prevent the paper sheets from twisting owing to its hardness in the axial direction. In addition, silicone 1, which is on the bottom of the soft chamber as a support, guarantees adequate resistance against the tendon force to the tendon path and reduces sinking of the sucker surface, making it in flat contact with objects. Silicone 2, serving as a layer of the jamming cavity, is soft and easy to deform, which allows effortless bending under the tendon-driven method.

Finite Element Simulation

Finite element method model

In this section, based on the finite element software ABAQUS, we use the finite element method (FEM) to analyze the mechanical properties of the finger.

The FEM model consists of four parts: silicone, steel layers, paper layers, and the rope. Solid (C3D8R), shell (S4R), and truss elements (T3D2) were used to simulate the silicone, steel (or paper) layer, and the rope portions,

MULTIMODE GRASPING

respectively. The contact type between layers is surface-to-surface contact, and the sliding formulation is finite sliding. The Ogden model was applied for the silicone portion,⁴⁴ and the strain energy potential U was expressed by

$$U = \sum_{i=1}^N \frac{2\mu_i}{\alpha_i} (\lambda_1^{\alpha_i} + \lambda_2^{\alpha_i} + \lambda_3^{\alpha_i} - 3) \quad (6)$$

where λ_i represents deviatoric principle stretches, and $N=3$, $\alpha_1=1.55$, $\mu_1=107.9 \times 10^3 \text{ J} \cdot \text{m}^{-3}$, $\alpha_2=7.86$, $\mu_2=21.47 \text{ J} \cdot \text{m}^{-3}$, $\alpha_3=-1.91$, and $\mu_3=-87.1 \times 10^3 \text{ J} \cdot \text{m}^{-3}$.

Experimental values of the material parameters of the layers were used in the simulation. The Young's modulus and Poisson's ratio of the steel and paper layers are $E_s=20.6 \text{ GPa}$, $\nu_s=0.3$ and $E_p=6 \text{ GPa}$, $\nu_p=0.2$, respectively. The coefficient of friction between the steel and steel layers, steel and paper layers, and paper and paper layers is 0.0, 0.1, and 1.3, respectively. The material parameters of the rope are the same as those of the steel layers.

Bending deformation simulation

To explore the relationship between deformation of the finger and displacement of the rope, several simulations were conducted. In this process, no gas was removed from the cavity of the silicone, and the gas pressure in the cavity was equal to 1.0 bar. Displacements were applied to the end point of the rope.

Different bending shapes of the finger under different displacements are shown in Figure 2A. The results show that with an increase in the displacement of the rope, the bending deformation of the finger becomes larger, as shown in Figure 2B. In addition, the FEM and experimental results are in good agreement when the displacement is small. However, when the displacement increases, the two results differ. The pulling force in the rope becomes larger when the deformation increases, and the rope sinks into the silicone at the fingertip; hence, the actual displacement and deformation are smaller than what the FEM result suggests. In addition, the bending shapes of the finger are similar to circular shapes. As shown in Figure 2A, bending deformation mainly occurs in the middle section. The coordinates of the FEM elements at the central line of the middle section after deformation are plotted in Figure 2C, and we found that the deformation shapes exhibit good agreement with circular shapes. The maximum strain occurs at $d=30 \text{ mm}$ in Figure 2A, and the maximum principal logarithmic strain is 0.36.

Variable stiffness simulation

To analyze the changes in the stiffness of the finger under different vacuum pressures in the cavity, forces were exerted on the end point of the finger and displacements of the end point were obtained.

Four conditions were considered in the experiment and FEM analysis, and the vacuum pressures were $p=0$,

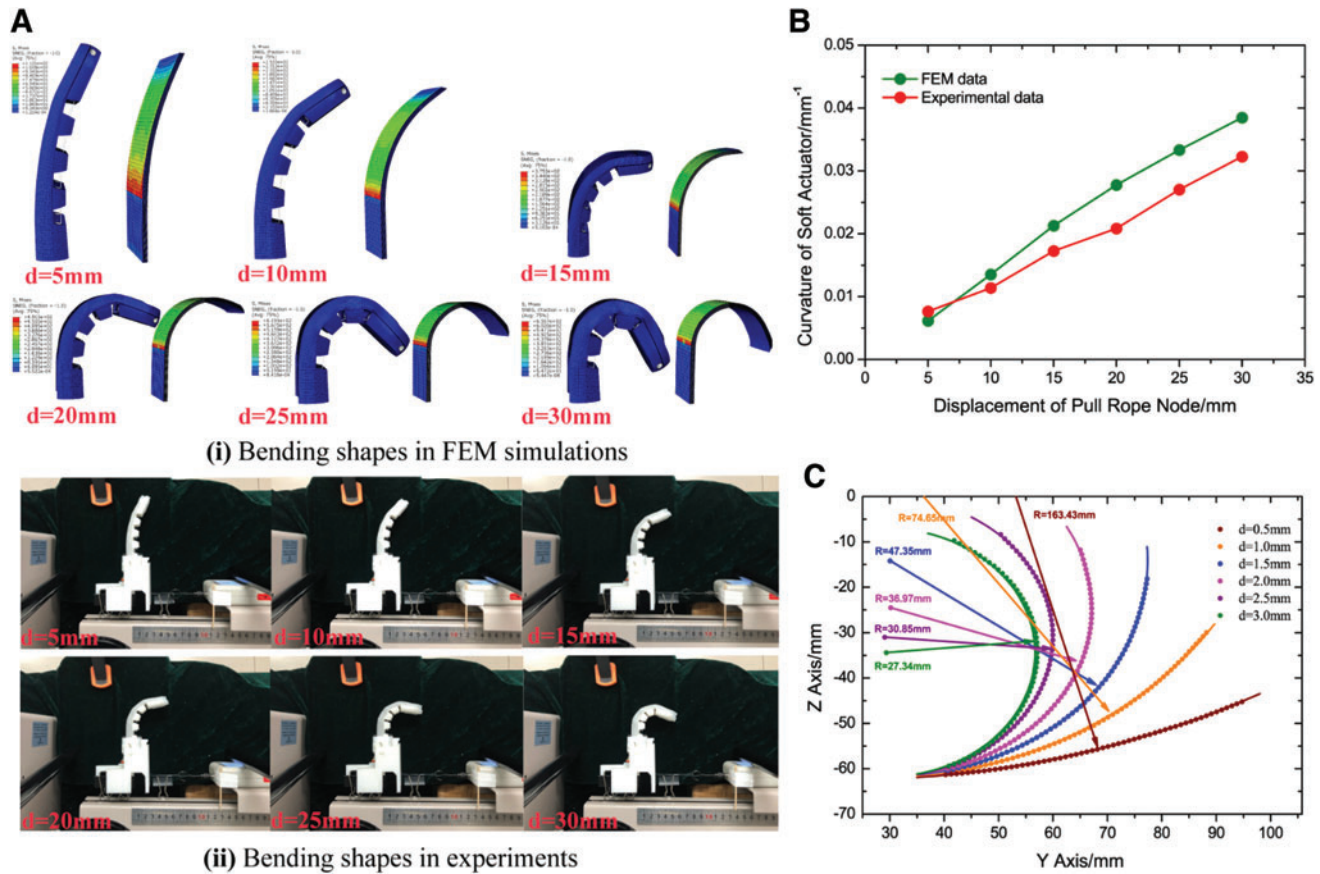


FIG. 2. Bending deformation. (A) Bending shapes under different displacements of the rope. (B) Deformation shapes of the middle section of the finger. (C) Radii of the finger under different displacements of the rope. Color images are available online.

– 0.025 MPa, – 0.050 MPa, and – 0.075 MPa. The results are shown in Figure 3A and B. We found that the displacements are different at different vacuum pressures for the same pulling force. The displacement decreases with an increase in the vacuum pressure, because the larger pressure value among the layers leads to higher stiffness of the finger.

Multimode Grasping Control

Control model of the finger

Movement of the rope knot results in flexuosity of the finger. While the rope knot is driven, the rope shifts and

shortens the length of the soft actuator, which bends toward the objects. Moreover, the relationship between the bending angle of the soft actuator and the displacement of the rope allows precise control. When the soft actuator bends, its grooves serve as a rotation structure. The bending deformation of all grooves generates the final bending state of the soft finger, as shown in Figure 4A. Such grooves were analyzed to obtain the relationship between the bending angle of the finger and the displacement of the rope. The schematic diagrams of the groove in different states are described as follows. There is a critical state for the groove when the broadsides of the grooves are perpendicular to the bottom

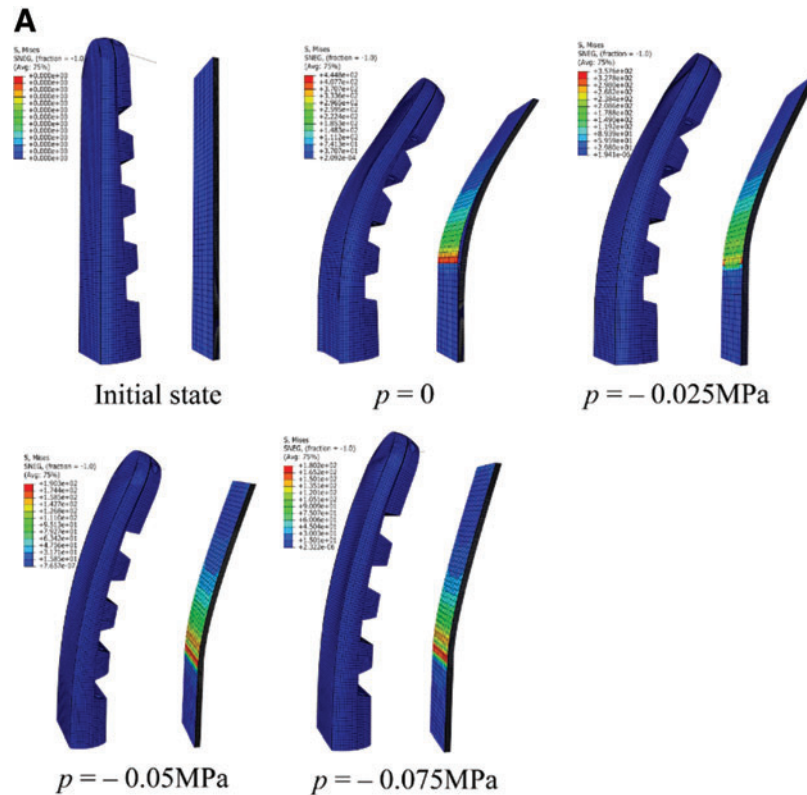
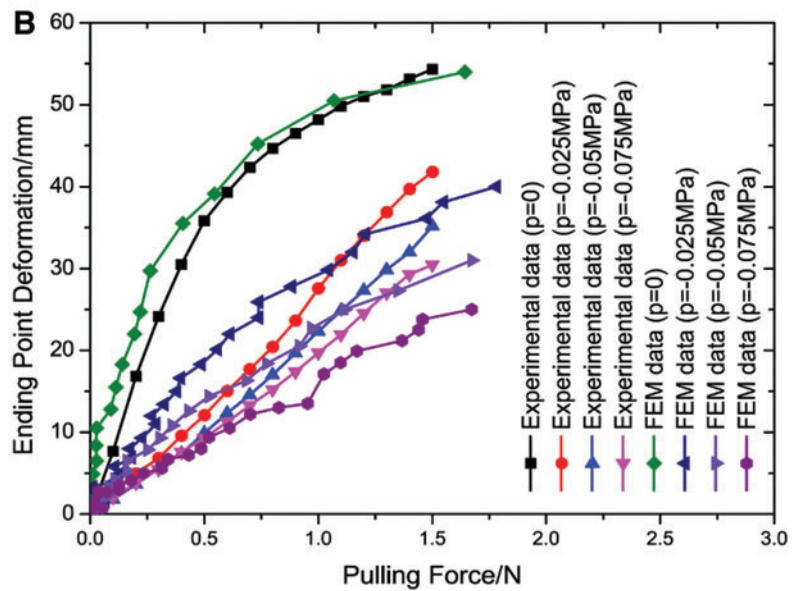


FIG. 3. Variable stiffness simulation. (A) Deformation shapes under different vacuum pressures. Pulling force $F \approx 1.7$ N. (B) Relationship between the displacement and the pulling force under different vacuum pressures. Color images are available online.



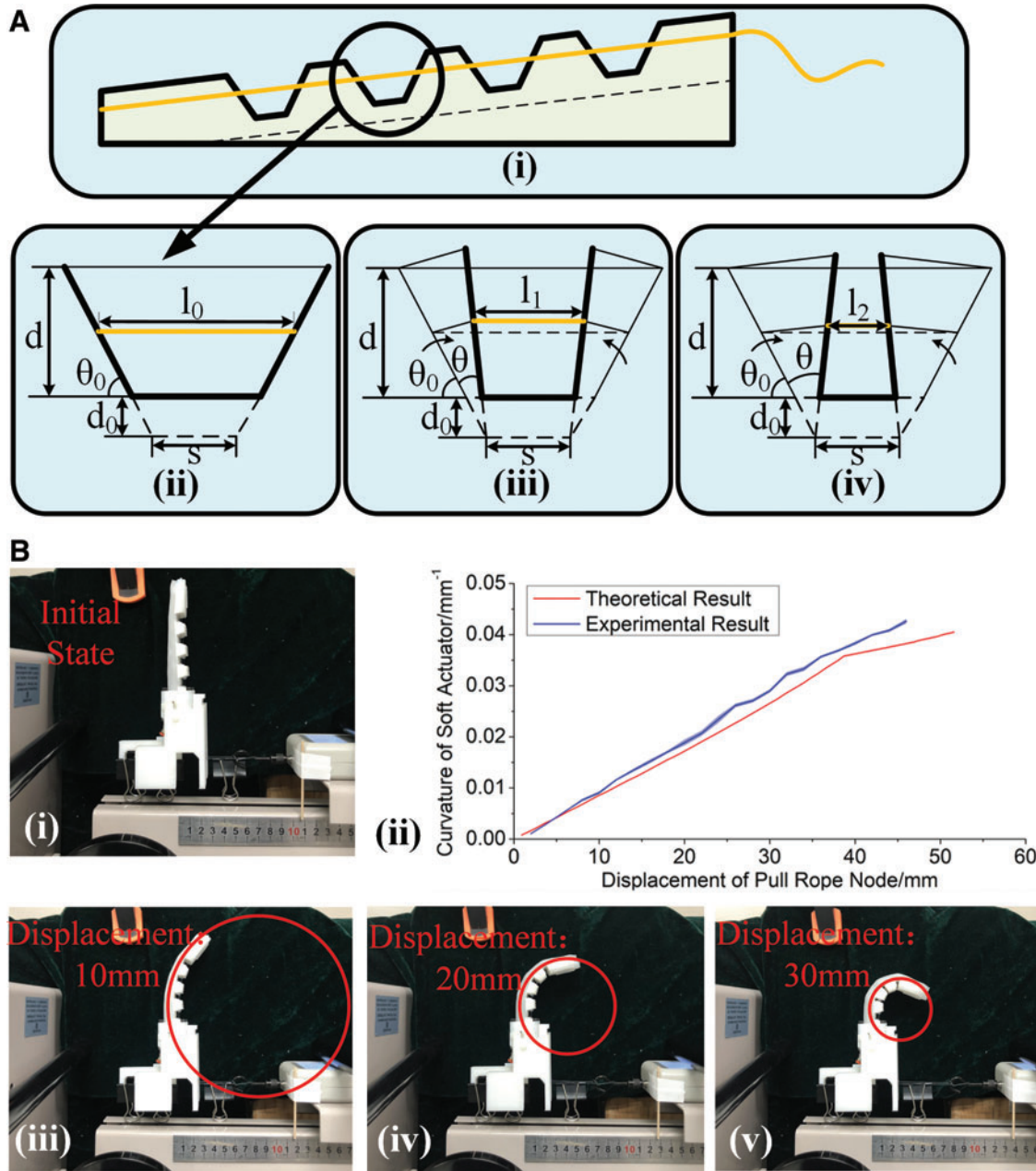


FIG. 4. Control model of the finger. (A) Bending deformation of the soft finger. (B) Comparison of the theoretical analysis and actual test. Color images are available online.

edge. The variation value of the tendon length in the groove can be calculated using Eqs. (7) and (8).

$$\Delta l = l_0 - l_1 = (2d_0 + d) \left(\frac{1}{\tan \theta_0} - \frac{1}{\tan(\theta_0 + \theta)} \right) \quad (7)$$

$$(\theta_0 + \theta) \leq 90^\circ$$

$$\Delta l = l_0 - l_2 = \frac{(2d_0 + d)}{\sin \theta_0} (\cos \theta_0 - \cos(\theta_0 + \theta)) \quad (8)$$

$$90^\circ \leq (\theta_0 + \theta) \leq 180^\circ$$

where Δl is the variable value of the tendon length in a groove, l_0 is the initial length of the tendon, and l_1 and l_2 are

the lengths of the tendon in a groove when bending before and after the critical state, respectively; θ_0 is the angle of the groove edge; and θ is the rotation angle of the edge of one side of the groove. When $\theta_0 + \theta$ equal 90° , this indicates a critical state. d and d_0 are the height of the groove and the distance from the bottom edge of the groove to the neutral surface of the finger, respectively, and s is the length of the groove's bottom edge on a neutral surface. s is a constant value and is always approximately processed as a straight line for simplification in the bending state.

The bending degree of the finger is quantized as a curvature, which can be calculated as a circle. The circle is obtained by three position points distributed on the neutral surface of the soft finger. The sum of all four Δl values of each groove is equal to the displacement of the rope in the

bending process. The red curve in Figure 4B(ii) shows the kinematic relationship between the rope displacement and its geometry curvature. The blue curve is the real curvature data, and it has an approaching trend with the red curve. Figure 4B(iii–v) indicates that with an increase in the displacement, the finger bends and the fitting circle of the body shows a lifting tendency. The curvature of the circles was measured using a picture processing method, showing that the actual test result is close to the theoretical results. The test platform is shown in Figure 4B(i), in which the finger is clamped on a pull-push platform, and a rule is attached along with the bearing of the platform. With the rotation of the hand crank, the displacement of the pulling rope and the displacement were measured by the rule, and each test result was recorded by a camera for image processing technologies to obtain the finger's curvature. With the rotation of the hand crank, the displacement of the rope was regulated by a dividing rule, and the results of the bending of the finger were determined.

Control strategy

Although the self-adaption of the finger realizes grasping of the SRG without damage to the object, the improper grasping mode and parameters hamper or even destroy the grasping stability. The self-adaption of the finger has an upper limitation, and overlarge parameters apply a stress to objects. An inadequate control mode hinders fingers from touching objects with a specific shape; for example, an enveloping grasp is incapable of lifting a piece of card on a desk. Based on the hardware system and direct executive components, such as the solenoid valve, vacuum pump, and motor tendon-driven mechanism (MTDM), there are three control modes such as an enveloping grasping mode (EGM), a clamping mode (CM), and a sucking mode (SM). Among them, the first two modes primarily involve two operation steps: (1) deformation operation by the MTDM; and (2) stiffness variation operation through the cooperation of the solenoid valve and vacuum pump. The last mode requires tight attachment of the sucker on the top of the finger to the surface of the object, and then the solenoid valve and vacuum pump are adjusted to create a negative pressure environment.

F5 ▶ As shown in Figure 5B, in the EGM, the motor pulls the tendon-driven mechanism to induce the gripper to wrap the objects tenderly and tightly, and then the solenoid valve and vacuum pump work together for stiffness. Based on the above steps, the motor continues to slightly mobilize the rotation pedestal, realizing a clamping force and enabling a powerful enveloping grasp for various objects. In this mode, the gripper is suited for grasping relative heavier, bigger, and more three-dimensional objects such as apple, boxes, and so on; when the soft actuators bend to stretch into a lifting handle, the gripper can hook some objects like a shopping bag and basket. As shown in Figure 5C, in the CM, the solenoid valve and vacuum pump cooperate to solidly pump the fingers in the original state. Then the rigid motion of the MTDM results in deformation of the finger to a small degree and also in a certain degree of rotation of the pedestal, making the fingertip converge to a point to pick up objects. Unlike the EGM, this grasping mode is similar to parallel pinching and allows clamping of pancake-type objects, as shown in Figure 5A(iii). Moreover, regardless of the mode, the move-

ment of the MTDM is controlled by the servo. The fingers can be in any position and state between the original and maximum deformation states according to practical applications. In the SM, the sucker first sticks to the surface of objects before the vacuuming operation, generating a vacuum adsorption effect, as shown in Figure 5A(iv). The SM has limited grab power but is good at adsorbing wafery-like objects, such as paperboard and cards, which are hard to clamp.

Different objects have different sizes, weights, and forms, thus requiring different appropriate control modes and control parameters to ensure a steady and effective grasp. For SRGs, only the underlying instructions, such as control modes and control parameters, are required to choose the mode and specific deformation outputs. SRGs only need to adjust the vacuum pump, speedy valve, and motor synchronously by real-time embedded system when switching between different modes. All these devices have a millisecond response time. The gripper needs no more than 2 s to switch from the initial mode to the three control modes and <0.5 s for all the other mode switch pairs.

Grasping performance

The combination of soft material and the tendon-driven method provides self-adaption ability to SRGs. As the main element of the gripper, soft material results in elastic physical contact with objects and reduces crash damage to the objects. Moreover, the tendon-driven method is a flexible and underactuated driving method with less constraint than a linkage-driven method. As shown in Figure 6A, four grooves **F6** can be elastically deformed together by changing the length of the only tendon in the finger. Although driven by the pulling force, the joint structures cannot maintain absolute immovability because of a lack of constraints, and the final bending state corresponds to the deformation combination of each of the grooves. The final bending is dependent on the length of the tendon and on the resistance force, which is applied to different positions of the finger. Therefore, when grasping different objects of different sizes and forms, the finger adopts different bending states under the same control parameters. This self-adaption ability allows the gripper to grasp light and soft objects without causing damage, but restricts the grasping power due to the lack of joint constraints.  shown in Figure 6B, an incompact rice ball is grasped but not broken, an elastic balloon can be wrapped without evident deformation, and plasticine remains nearly the same after being grasped. Figure 6B(iv and v) shows the same plasticine recorded before and after being grasped, and the two subgraphs indicate that the SRG can apply soft force to objects by adapting a bending state before strengthening the structure stiffness.

Heavy objects apply a powerful resistance force to the structure, affecting the bending state and leading to the loose of the grasping posture toward the objects, which results in unreliable grasping. The variable stiffness characteristic is an ideal treatment for optimizing adaptive grasping to grasp heavy objects. By changing the stiffness characteristic of the finger, a powerful constraint is added to the finger, and the SRG obtains a steady grasping posture when grasping objects. After the vacuum operation, the finger can be approximately rigid in structure.

MULTIMODE GRASPING

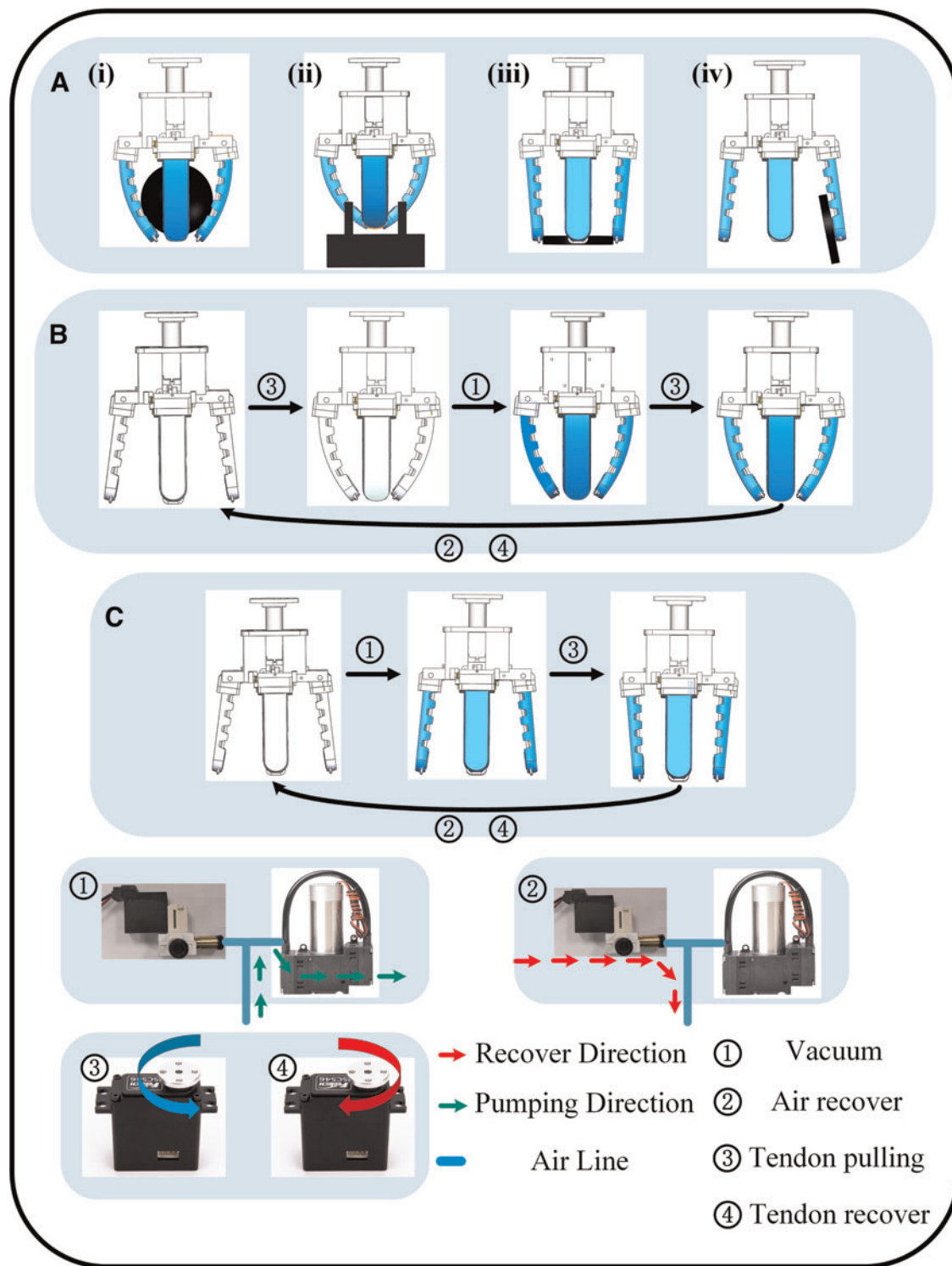


FIG. 5. Control strategy diagram. (A) Diagram of EGM for grasping and hooking, CM, and SM. (B) control process of EGM and (C) CM. CM, clamping mode; EGM, enveloping grasping mode; SM, sucking mode. Color images are available online.

Based on the mechanism features and driving method, the SRG exhibits anthropomorphic performance. The soft material constituting the finger has biological characteristics similar to human flesh, which allows a soft touch with objects, similar to human hands. Moreover, human hands can

grasp objects of various sizes and forms with steady self-adaptive grasping, which is analogous to the self-adaption ability of the SRG. Another anthropomorphic performance is shown in Figure 6C. The SRG uses the enveloping grasp to grab an apple, uses the clamp grasp to clamp a wet wipes

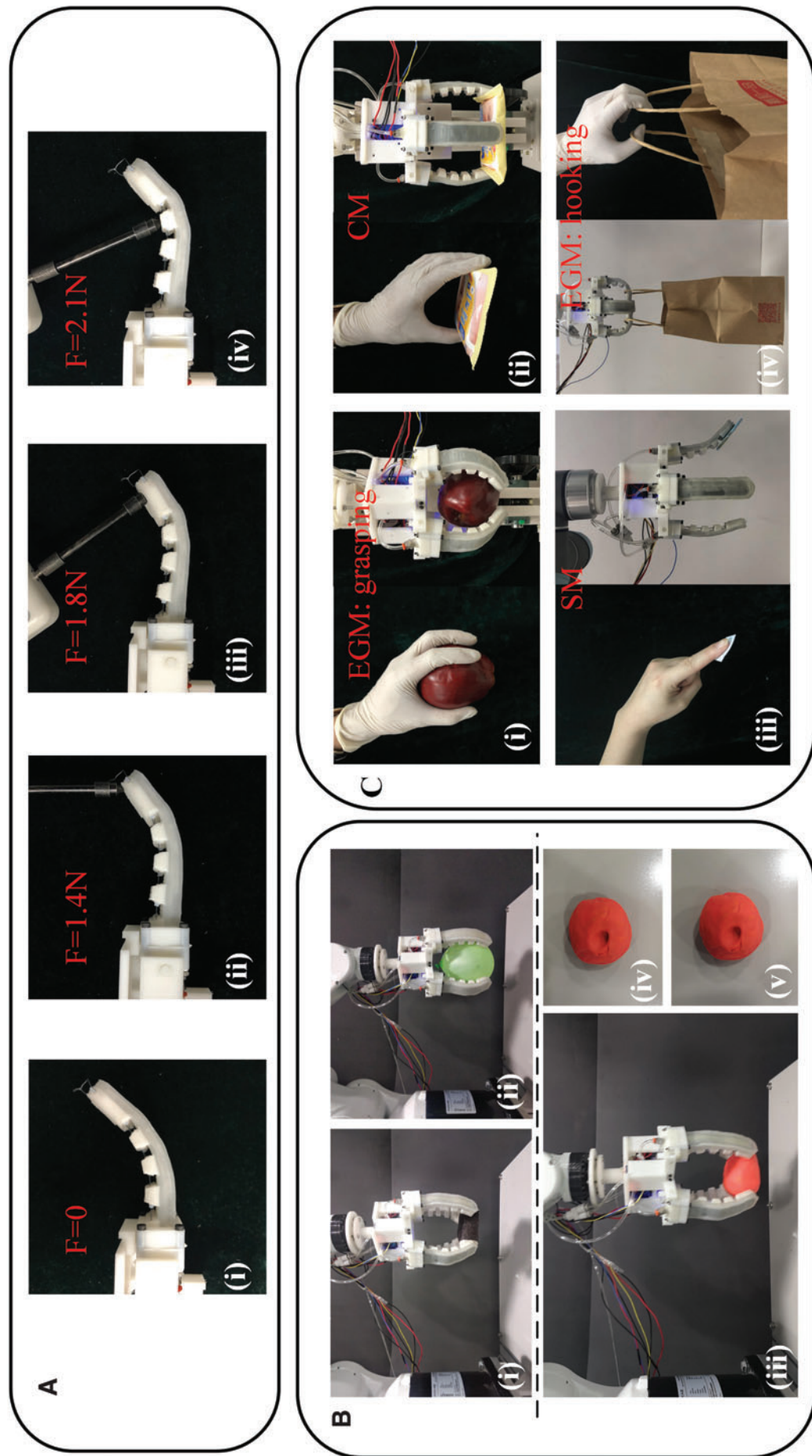


FIG. 6. Grasping performance. (A) All fingers are in a bending state under the same tendon displacement. (B) Self-adaption ability of the gripper. (C) Anthropomorphic human hand grasping skills with several grasping modes. Color images are available online.

package, adopts the fingertip to adhere to a small piece of paper, and utilizes the enveloping grasp to hook a sack. The above motions imitate those of the human hand with several grasping modes.

The grasping process in humans is divided into several events: (1) closing of the fingers to enclose an object without damaging it; (2) intensification of the joint muscles of the fingers to support the weight of the object; and (3) application of a clamping force to the object to generate friction force.

These operations are simulated by the SRG, which uses three similar operations: (1) closing of the fingers to enclose an object; (2) stiffening to bear the weight of the object; and (3) driving of the tendon-driven mechanism for pedestal rotation to generate a clamping force. For the second operation, the stiffness improvement of the finger corresponds to the working of the finger joint muscles. The clamping force in the grasping process contributes to the elevation of the friction force between the fingertips and the object surface, which always occurs in human grasping operations. The similarities in material, self-adaptation ability, multimode, and grasping processes between the human hand and the proposed gripper illustrate the anthropomorphic performance of the SRG. This anthropomorphic performance is conducive to the direct transfer of human grasping skills to the gripper.

Experiments

Variable stiffness experiment

The improvement in the stiffness of the finger provides improved ability to prevent deformation. This ability is important in supporting grasped objects; thus, it is meaningful to test the specific variable stiffness performance. A pull-push tension meter platform was built to test the variable stiffness performance. The platform includes a tension meter with 0.01 N precision mounted on a pull-push platform's mobile station, a 3D-printed fixture clamping the finger, and a hardware testing system supplying a vacuum environment. A tendon tied the fingertip and tension meter. When the hand crank on the pull-push platform was rotated, the tension meter had a tendency to pull the end point of the finger by the tendon. With an increase in displacement of the tension meter, the pulling force resulted in incremental stress to the finger, leading to an increasing end point deformation of the finger. When the hand crank was rotated back, the pulling force was gradually withdrawn. The pulling force loading cycle (loading pulling force->unloading->reloading) was also completed to verify the hysteresis phenomenon. A rule with 1 mm precision fixed on the pull-push platform was used to obtain accurate measurement results to the millimeter level, which meets the demand to distinguish and weigh the data difference among variable pulling forces.

The results are recorded by three experiments, and the final data with standard deviation of three repetitions are shown in **F7** ▶ Figure 7B. In loading stage, when the finger is in a stiff state, the pulling force produces a considerably smaller end point deformation than the soft state. The red curve with a triangle indicates the horizontal displacement of the finger end point, which is in a soft state when a horizontal pulling force is applied. When the pulling force is higher than 0.3 N, the horizontal displacement value exhibits nonlinear growth because the overlarge bending deformation is not able to maintain the pulling force direction perpendicular to the

contact surface of the ending point. The blue curve, which has a smaller fitting slope, shows that horizontal displacement strengthening of the stiffness improves the ability to resist deformation. The hysteresis phenomenon exists and is caused by the layer slide under the external pulling force. The slide changes the relative position between layers, and the friction forces the jamming structure from reshaping into a new form.

As the curves shown in Figure 7, the maximal variable stiffness ratio is ~ 6.02 times, which is evaluated by the average of the deformation distance's multiple between the stiff and soft states at 0.20, 0.22, 0.24, ..., 0.76, 0.78, and 0.8 N pulling force, respectively. As shown in Figure 7E and F, the finger has less deformation in the stiff state than in the soft state. When gradually unloading, stiff-state finger cannot recover to the original upright state when the soft-state finger is not accompanied by the hysteresis phenomenon. It is reasonable to consider that the slight slip of the layer materials in the deformation process results in a curve reshape for the vacuumed finger until the fingers turn to a soft state.

Pulling conversion efficiency experiment

The finger-grasping power has a direct influence on grasping stability. Under a limited pulling force, the force transmission efficiency is the main determinant of the grasping power. In real applications, the fingers can be controlled in any feasible bending state according to the object. To explore the force transmission efficiency of the fingers in different bending states, another tension meter tied to the pulling tendon ending was added to the testing platform. In the test, the tendon tied to the fingertip was kept tense and perpendicular to the contact surface of the end point at all times. Before testing, the finger was adjusted to different bending degrees, including 0°, 30°, 60°, and 90°. After the vacuum operation, the finger maintained its bending state, and the pulling force from the tension meter was gradually increased. The stress on the fingertip when applying a pulling force was collected from the tension meter. As shown by the average results with standard deviation of three repetitions in Figure 8A, the bending degree of the end point contact surface was primarily adjusted from 0° to 90°, which is the frequently used bending degree range of the finger. The results indicate that the larger the bending deformation of the finger, the higher the transmission efficiency of the pulling force. The ratio of the average transmission efficiency is 8.1%, 8.5%, 11.4%, and 22% at 0°, 30°, 60°, and 90° bending states, respectively, indicating that the SRG can acquire more powerful grasping strength when the finger is in a larger deformation state. **F8** ◀

Grasping power experiment

To test the grasping, clamping, and sucking power of the proposed gripper, an experimental platform was built based on the pull-push platform, as shown in Figure 8B. A soft gripper was fixed on a mobile station on the top of the pull-push platform. The UART port was used to transmit the control signal from the computer. A force sensor and grasping force transmit device (GFTD) were fixed together on the bottom of the pull-push platform, and the above three devices were kept in a perpendicular line. The vacuum pump was placed on the platform and connected to the total pneumatic input and output port of the SRG, providing a vacuum source for the variable stiffness function. The force sensor was

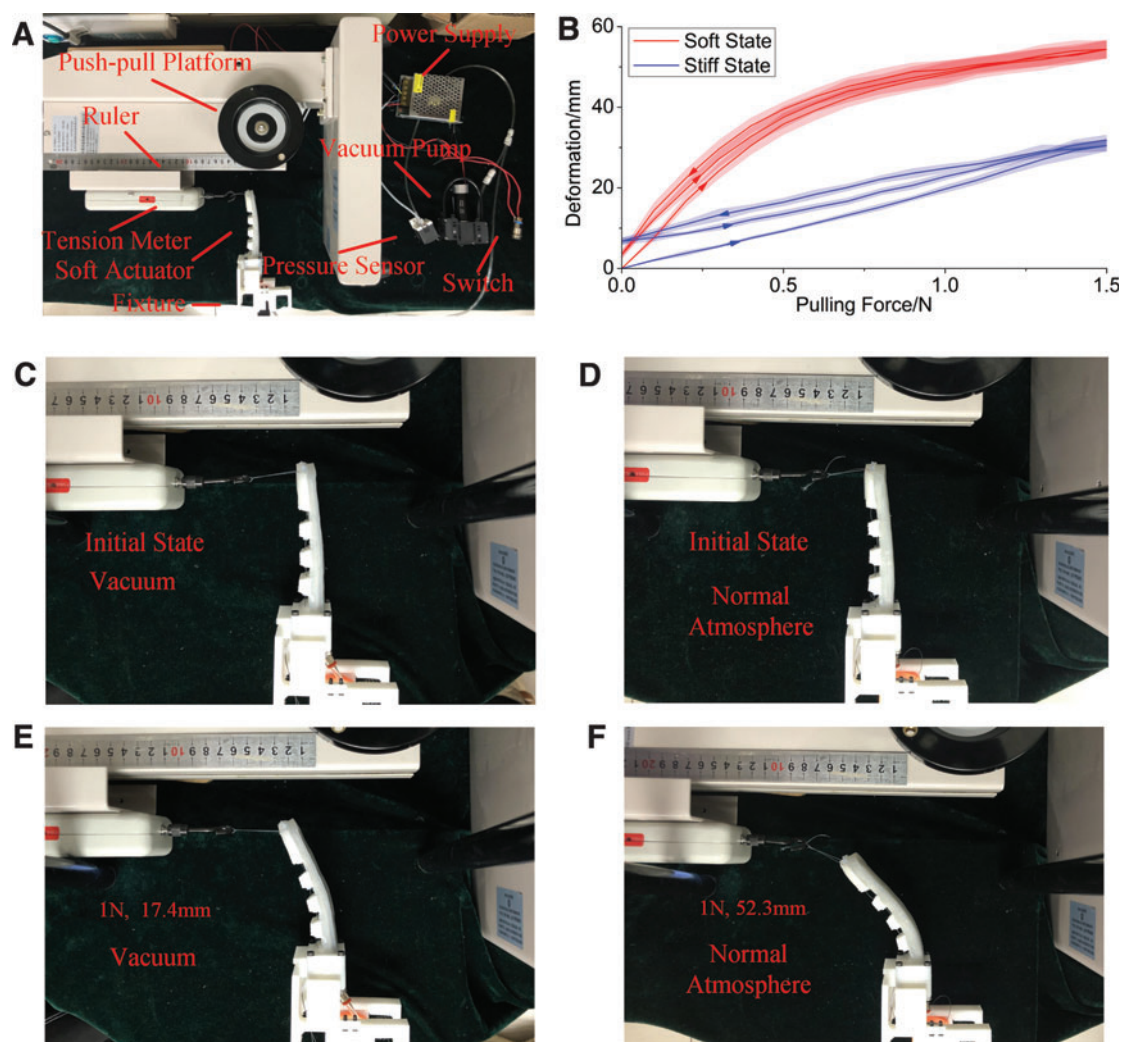


FIG. 7. Variable stiffness experiment. (A) Testing platform, including a push-pull platform, tension meter, power source, pressure sensor, and vacuum pump. (B) Comparison of the end point deformation between a stiff and a soft state under the same pulling force on the tip, and the *arrow* direction represents the pulling force vary direction. Initial state of the finger under a (C) stiff and (D) soft state. Deformation results when a 1 N pulling force is applied to the finger under a (E) stiff state and (F) soft state. Color images are available online.

connected to a sensor transmitter, and the force signals were sent to the computer through a 485 port.

When measuring the grasping power of the gripper, the gripper was adjusted to envelope and grasp a bowl-shaped GFTD, as shown in Figure 8C(v). Then, the hand crank on the pull-push platform was rotated to generate a rise in the mobile station. As the mobile station rose, a grasping force was generated to hold onto the GFTD as much as possible. The results of each process were recorded by a force sensor thrice and uploaded to the PC. Then, grasping power, sucking power, and clamping power tests were implemented and handled in the same way. When the displacement of the mobile station exceeded the deformation of the fingers, which were not able to produce an effective upward force, the force started to decline. The peak force value was a comparable representation of the grasping power. To compare the variable stiffness effect, the finger was assessed in a stiff and soft state in succession, and as shown by the curves with standard deviation of three repetitions in Figure 8C(i), the peak force value in the stiff state increased to 31.06 N but 20.64 N in

the soft state. The LJS provided 50.48% peak grasping power improvement. Moreover, a rectangular GFTD (shown in Fig. 8C[vi]), which is appropriate for the sucking power test, replaces the bowl-shaped GFTD. A similar test process was executed until the sucking force started to decrease. The difference was that the gripper only sucked the surface of the GFTD without providing chucking power. Figure 8C(ii) displays the results of the sucking power test, with the peak force exceeding 40 N under the combined action of four suckers. A clamping power test was similarly performed, and the gripper was set into CM. As shown in Figure 8C(iii), the CM output exhibited the weakest grip power.

Therefore, only stabilized grasping is useful, and an excessive increasing in the gripper results in moderate finger deformation, which deteriorates the grasping stability. A small rising distance is valuable, and thus, only force data under 5, 10, 15, 20, and 25 mm distances were recorded without considering larger values. On the basis of the test platform, the value of the rising distance was understood as the antideformation ability when grasping, sucking, or

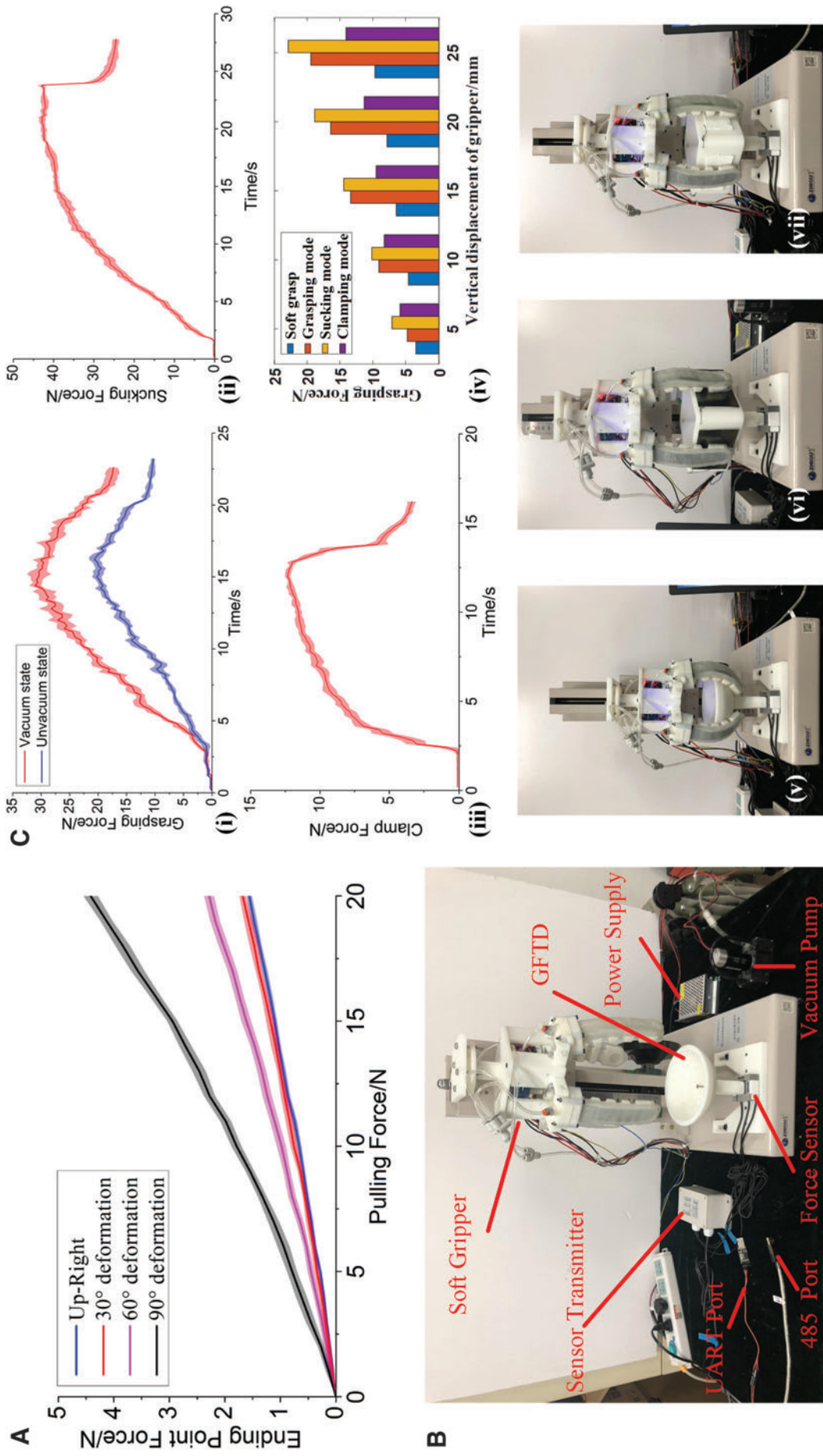


FIG. 8. Experiments of pulling conversion efficiency and grasping power. (A) Test results of pulling force transmission efficiency. (B) Platform to test the grasping power of the proposed gripper. (C) Grasping power test of the gripper using the EGM, SM, and CM: (i) comparison of the actual results between the stiff state and soft state if the SRG is operated in the EGM. (ii) Sucking force test results of the SRG in the SM. (iii) Clamping force test results of the SRG in the CM. (iv) Results indicating grasping force under different rising distances for three types of grasping mode. (v-vii) Testing scenes for the three grasping modes. SRG, soft robotic gripper. Color images are available online.

clamping a specific object. Under a specific gripping object, the less the rising distance, the more powerful and stable the gripper output. To measure the effective maximal grip power of the gripper, the force data were recorded when the rising distance of the gripper was 5, 10, 15, 20, and 25 mm in soft grasp state, EGM, SM, and CM. As displayed by the average results in blue and red bar in Figure 8C(iv), contrast to the soft grasp state without vacuum operation, EGM has 38.18% (5 mm vertical displacement), 97.86% (10 mm), 108.39% (15 mm), 110.01% (20 mm), and 101.15% (25 mm) grasping power output promotion.

Grasping experiment

The variable stiffness of the proposed SRG allows multi-mode grasping. As the main component of the gripper, the

soft material provides the gripper the ability to grasp without causing damage, and the variable stiffness performance enhances its ability to lift heavy objects. In real life, different objects have various sizes, weights, and shapes and require appropriate grasp modes and skills. As shown in Figure 9, the gripper adopts the EGM (vertical/horizontal grasp direction and hook take), CM, and SM to grasp different daily objects. Therefore, the proposed SRG was verified to be adaptable and exhibited multimode grasping of objects with various shapes, sizes, and weights.

The grasp steps of the four grasping modes are shown in Figure 5, and photos of the SRG grasping objects are presented in Figure 10. Four types of objects were selected to be grabbed according to the target grasp mode. Figure 10A–D illustrates the enveloping grasp, clamp grasp, hook grasp, and suck grasp processes.

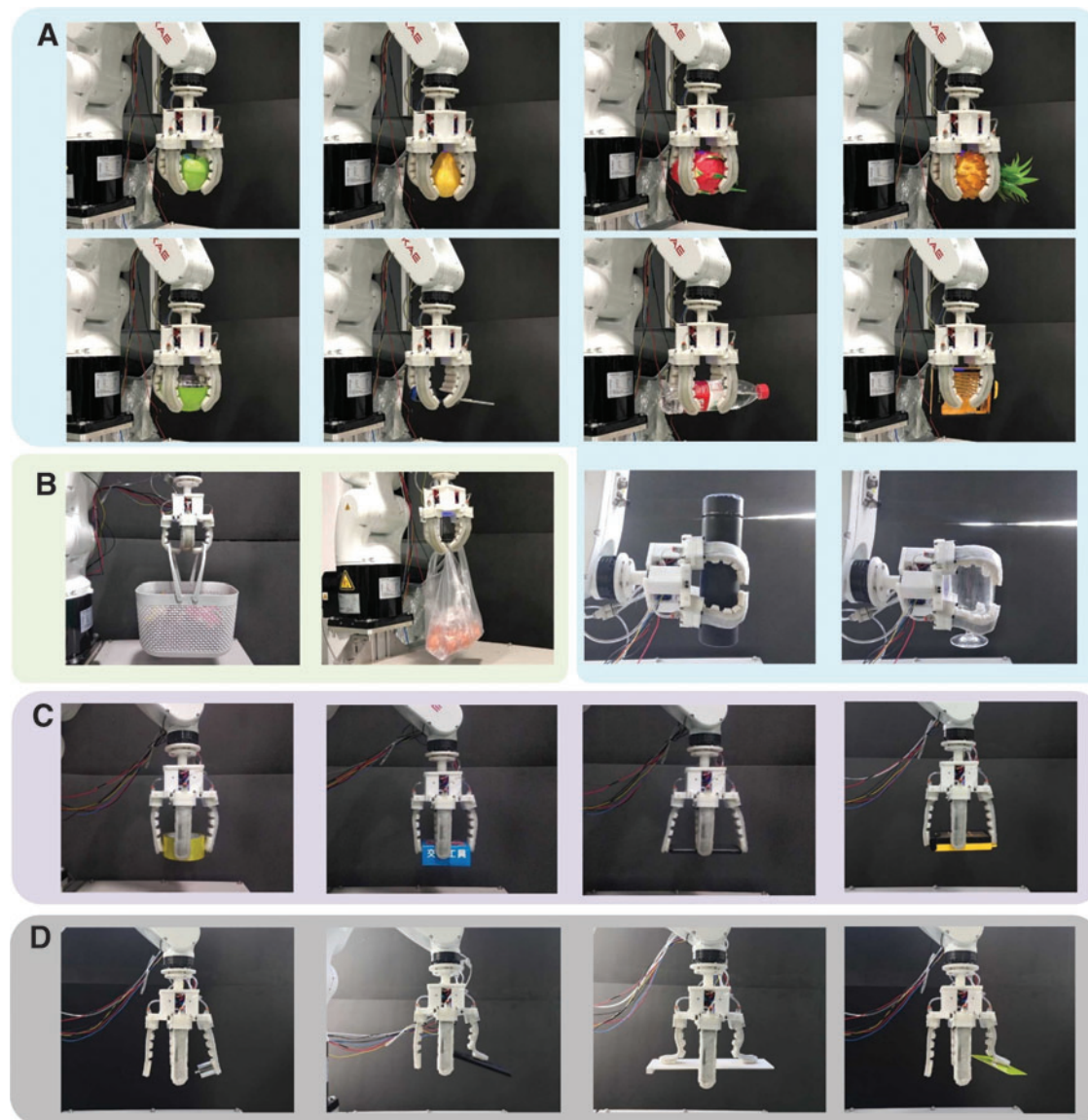


FIG. 9. Nineteen types of objects are grasped using different grasp modes. (A) Use EGM to grasp an apple, pear, pitaya, pineapple, bowl, screwdriver, plastic water bottle, tool box and grasp a vacuum cup, glass cup in the horizontal direction, respectively. (B) Use EGM to hook up a basket and plastic bag with eggs, respectively. (C) Use CM to grasp a packaging tape, paper box, mobile phone, and tool box, respectively. (D) Use SM to suck up a weight, mobile phone, slab, and card, respectively. Color images are available online.

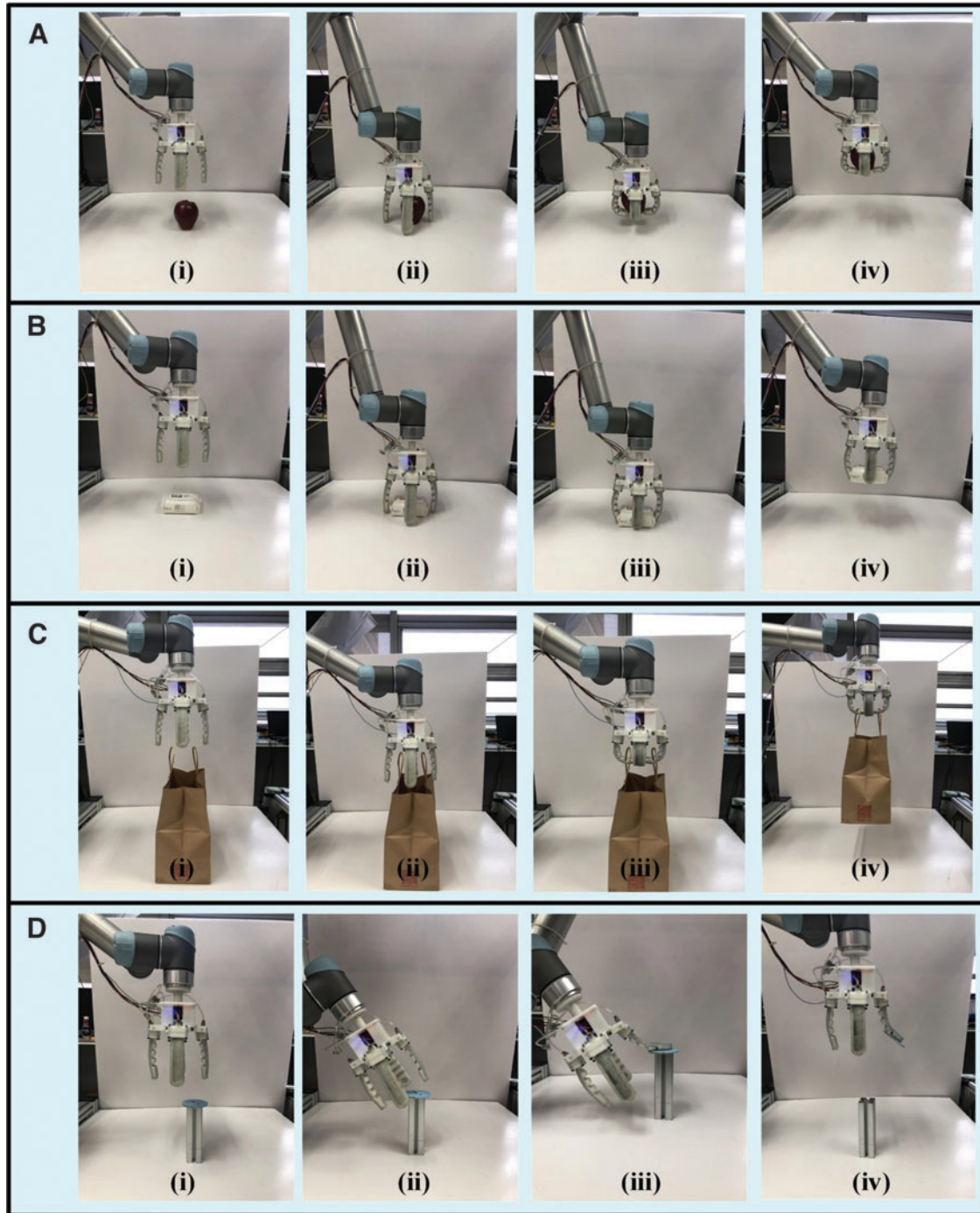


FIG. 10. Operation steps of four grasping modes. (A) grasping, (B) clamping, (C) hooking, and (D) sucking operation steps. Color images are available online.

Discussion

The above experiments were implemented to verify the performance of the proposed gripper. To confirm the accuracy between the bending curvature of the finger and the displacement of the rope knot, a comparison test was designed. The simplified geometry mode is close to the real test results, with a 0.0024 mm^{-1} curvature average error. To test the variable stiffness performance, a pull-push tension meter platform was built to compare the resistance variation degree.

The test results show an ~ 6.02 times stiffness enhancement when a 0.75 vacuum degree is applied to the layer jamming cavity. In the pulling conversion efficiency experiment, after vacuuming under different bending states, the soft finger reveals that 90° , 60° , 30° , and 0° bending exhibits 22.0%, 11.4%, 8.5%, and 8.1% transmission efficiency of pulling force, respectively. In addition, using a pressure measurement sensor, we obtained dynamic curves recording the grasping force variation in soft grasp state, EGM, SM, and CM. There is 50.48% peak grasping power improvement and

38.18% (5 mm vertical displacement), 97.86% (10 mm), 108.39% (15 mm), 110.01% (20 mm), and 101.15% (25 mm) grasping power output promotion between soft grasp state and EGM. Regarding the multimode grasping ability, the proposed SRG uses several grasping modes to adaptively grasp objects of various shapes, sizes, and weights. The tests above prove the paper as layer jamming material meeting the stiffness improvement requirement and helping the gripper strengthen the grasping power to a certain extent. With the help of the jamming structure, the proposed soft gripper realizes multimode grasping under flexible control sequential, and it verifies that the novel multimode grasping ability for soft gripper is effective.

Conclusion

This study presents the design, analysis, and experiments of a tendon-driven soft gripper with a layer jamming variable stiffness structure. The combination of a tendon-driven approach and LJS integrates soft and multimode grasping. Under the cooperative control of vacuum devices and a tendon-driven structure, the gripper can realize compliant grasping and multimode grasping modes, including enveloping grasping, clamping, sucking, and hooking. The EGM is suitable for grasping and hooking, and the CM and SM can be adjusted to handle different sizes, shapes, and weights. For objects with stereo forms, such as a ball, bottle, and fruits, the EGM is an appropriate grasping mode to smoothly lift the object. For oblate or small objects, such as a mobile phone, box, book, or ping-pong ball, the CM is effective. For thin objects, such as a card or a slab, the SM is irreplaceable. Objects with a pothook can be hooked in the EGM. The multimode grasping performance of the proposed gripper expands the range of objects that can be grasped. The experimental results verify the self-adaptation ability, multimode grasping capacity, and anthropomorphic performance of the proposed SRG.

The multimode grasping ability is the novelty of our soft gripper, and this characteristic expands the objects' graspable types and shapes. Soft grippers often focus on soft and compliant grasping but ignore multimode grasping, which simplifies the design and control but limits the application. Variable stiffness ability is a meaningful performance for soft gripper and it can be excavated for more value. The soft gripper with compliant grasping, variable stiffness ability, and multimode grasping ability is a feasible and meaningful research point.

AU7 ► Author Disclosure Statement

No competing financial interests exist.

Funding Information

This work was supported by the National Natural Science Foundation of China (grant no. 91848206) and Tsinghua University Department of Computer Science and Technology-Siemens Ltd., China Joint Research Center for Industrial Intelligence and Internet of Things.

References

1. Yap YL, Sing SL, Yeong WY. A review of 3D printing processes and materials for soft robotics. *Rapid Prototyp J* 2020;26:1345–1361.
2. Galloway KC, Chen Y, Templeton E, *et al.* Fiber optic shape sensing for soft robotics. *Soft Robot* 2019;6:671–684.
3. Bao G, Fang H, Chen L, *et al.* Soft robotics: academic insights and perspectives through bibliometric analysis. *Soft Robot* 2018;5:229–241.
4. Laschi C, Cianchetti M. Soft robotics: new perspectives for robot bodyware and control. *Front Bioeng Biotechnol* 2014;2:1–5.
5. Galloway KC, Becker KP, Phillips B, *et al.* Soft robotic grippers for biological sampling on deep reefs. *Soft Robot* 2016;3:23–33.
6. Hao Y, Gong Z, Xie Z, *et al.* Universal soft pneumatic robotic gripper with variable effective length. In: 35th Chinese Control Conference (CCC), Chengdu, China, 2016, pp. 6109–6114.
7. Gao B, Yang S, Jin H, *et al.* Design and analysis of underactuated robotic gripper with adaptive fingers for objects grasping tasks. In: 2016 IEEE International Conference on Robotics and Biomimetics (ROBIO), Qingdao, China, 2016, pp. 987–992.
8. Shintake J, Caccuciolo V, Floreano D, *et al.* Soft robotic grippers. *Adv Mater* 2018;30:1707035.
9. Deimel R, Brock O. A novel type of compliant and underactuated robotic hand for dexterous grasping. *Int J Robot Res* 2016;35:161–185.
10. McEvoy MA, Correll N. Thermoplastic variable stiffness composites with embedded, networked sensing, actuation, and control. *J Compos Mater* 2015;49:1799–1808.
11. Ren T, Li Y, Xu M, *et al.* A novel tendon-driven soft actuator with self-pumping property. *Soft Robot* 2020;7:130–139.
12. In H, Lee H, Jeong U, *et al.* Feasibility study of a slack enabling actuator for actuating tendon-driven soft wearable robot without pretension. In: 2015 IEEE International Conference on Robotics and Automation (ICRA), Seattle, WA, USA, 2015, pp. 1229–1234.
13. Fei Y, Wang J, Pang W. A novel fabric-based versatile and stiffness-tunable soft gripper integrating soft pneumatic fingers and wrist. *Soft Robot* 2019;6:1–20.
14. Huang H, Wu L, Lin J, *et al.* A novel mode controllable hybrid valve pressure control method for soft robotic gripper. *Int J Adv Robot Syst* 2018;15:1729881418802140.
15. Katzschmann RK, Marchese AD, Rus D. Hydraulic autonomous soft robotic fish for 3D swimming. In: Hsieh M, Khatib O, Kumar V (Eds). *Experimental Robotics*. Cham: Springer, 2016, pp. 405–420.
16. Lau GK, Heng KR, Ahmed AS, *et al.* Dielectric elastomer fingers for versatile grasping and nimble pinching. *Appl Phys Lett* 2017;110:182906.
17. O'Halloran A, O'malley F, McHugh P. A review on dielectric elastomer actuators, technology, applications, and challenges. *J Appl Phys* 2008;104:071101.
18. Wang W, Ahn SH. Shape memory alloy-based soft gripper with variable stiffness for compliant and effective grasping. *Soft Robot* 2017;4:379–389.
19. Aukes DM, Heyneman B, Ulmen J, *et al.* Design and testing of a selectively compliant underactuated hand. *Int J Robot Res* 2014;33:721–735.
20. Hou X (Ed). *Design, Fabrication, Properties and Applications of Smart and Advanced Materials*. CRC Press, 2016. ◀ AU8
21. Sun T, Chen Y, Han T, *et al.* A soft gripper with variable stiffness inspired by pangolin scales, toothed pneumatic actuator and autonomous controller. *Robot Comput Integr Manuf* 2020;61:101848.

22. Behbahani SB, Tan X. Design and dynamic modeling of electrorheological fluid-based variable-stiffness fin for robotic fish. *Smart Mater Struct* 2017;26:085014.
23. Pettersson A, Davis S, Gray JO, *et al.* Design of a magnetorheological robot gripper for handling of delicate food products with varying shapes. *J Food Eng* 2010;98:332–338.
24. Yufei H, Tianmiao W, Xi F, *et al.* A variable stiffness soft robotic gripper with low-melting-point alloy. In: *IEEE 36th Chinese Control Conference (CCC)*, Dalian, China, 2017, pp. 6781–6786.
25. Shan W, Lu T, Majidi C. Soft-matter composites with electrically tunable elastic rigidity. *Smart Mater Struct* 2013;22:085005.
26. Yang Y, Chen Y, Wei Y, *et al.* Novel design and three-dimensional printing of variable stiffness robotic grippers. *J Mech Robot* 2016;8:061010.
27. Al-Rubaii M, Pinto T, Qian C, *et al.* Soft actuators with stiffness and shape modulation using 3D-printed conductive polylactic acid material. *Soft Robot* 2019;6:318–332.
28. Narang YS, Vlassak JJ, Howe RD. Mechanically versatile soft machines through laminar jamming. *Adv Funct Mater* 2018;28:1707136.
29. Lin KY, Gupta SK. Soft fingers with controllable compliance to enable realization of low cost grippers. In: *2017 Conference on Biomimetic and Biohybrid Systems*. Springer, Cham, 2017, pp. 544–550.
30. Jiang P, Yang Y, Chen MZQ, *et al.* A variable stiffness gripper based on differential drive particle jamming. *Bioinspir Biomim* 2019;14:036009.
31. Christoph K, Ian W, Olaf T, *et al.* Experimental and numerical analysis of fiber matrix separation during compression molding of long fiber reinforced thermoplastics. *J Compos Sci* 2017;1:2–18.
32. Bryan P, Kumar S, Sahin F. Tunable anisotropic stiffness with square fiber jamming. In: *2020 IEEE International Conference on Soft Robotics (RoboSoft)*, New Haven, USA, 2020, pp. 879–884.
33. Wang T, Zhang J, Li Y, *et al.* Electrostatic layer jamming variable stiffness for soft robotics. *IEEE/ASME Trans Mech* 2019;24:424–433.
34. Yang Y, Zhang Y, Kan Z, *et al.* Hybrid jamming for bio-inspired soft robotic fingers. *Soft Robot* 2020;7:292–308.
35. Ou J, Yao L, Tauber D, *et al.* JamSheets: thin interfaces with tunable stiffness enabled by layer jamming. In: *Proceedings of the 8th International Conference on Tangible, Embedded and Embodied Interaction*, New York, USA, 2014, pp. 65–72.
36. Wall V, Deimel R, Brock O. Selective stiffening of soft actuators based on jamming. In: *2015 IEEE International Conference on Robotics and Automation (ICRA)*, Seattle, USA, 2015, pp. 252–257.
37. Zhu M, Mori Y, Wakayama T, *et al.* A fully multi-material three-dimensional printed soft gripper with variable stiffness for robust grasping. *Soft Robot* 2019;6:507–519.
38. Gao Y, Huang X, Mann IS, *et al.* A novel variable stiffness compliant robotic gripper based on layer jamming. *J Mech Robot* 2020;12:051013.
39. Wang Z, Torigoe Y, Hirai S. A prestressed soft gripper: design, modeling, fabrication, and tests for food handling. *IEEE Robot Autom Lett* 2017;2:1909–1916.
40. Zhong G, Hou Y, Dou W. A soft pneumatic dexterous gripper with convertible grasping modes. *Int J Mech Sci* 2019;153:445–456.
41. Bryan P, Kumar S, Sahin F. Design of a soft robotic gripper for improved grasping with suction cups. In: *2019 IEEE International Conference on Systems, Man and Cybernetics (SMC)*, Bari, Italy, 2019, pp. 2405–2410.
42. Wang Z, Or K, Hirai S. A dual-mode soft gripper for food packaging. *Robot Auton Syst* 2020;125:103427.
43. Oliver-Butler K, Till J, Rucker C. Continuum robot stiffness under external loads and prescribed tendon displacements. *IEEE Trans Robot* 2019;35:403–419.
44. Elsayed Y, Vincensi A, Lekakou C, *et al.* Finite element analysis and design optimization of a pneumatically actuating silicone module for robotic surgery applications. *Soft Robot* 2014;1:255–262.

Address correspondence to:

Fuchun Sun
 Tsinghua National Laboratory
 for Information Science and Technology
 Department of Computer Science and Technology
 Tsinghua University
 Beijing 100084
 China

E-mail: fcsun@mail.tsinghua.edu.cn

AUTHOR QUERY FOR SORO-2020-0065-VER9-FANG_1P

AU1: Please identify (highlight or circle) all authors' surnames for accurate indexing citations. correct

AU2: Please confirm the correctness of authors' affiliations. correct

AU3: Please mention division or department, if any, in authors' affiliations 2–4 and corresponding author's address. The word of "School" and "Institute" can be revised as department.

AU4: Keywords have been taken from PDF. Please check. No problem

AU5: The Publisher requests for readability that no paragraph exceeds 15 typeset lines. Please check for long paragraphs and divide where needed. I have added the marks in the long paragraphs.

AU6: Please expand "PET." Polyethylene terephthalate

AU7: Disclosure Statement accurate? If not, please amend as needed. Correct

Hou X. Design, Fabrication, Properties and Applications of Smart and Advanced Materials. CRC Press, 2016, 10.1201/b19977:230-274.

AU8: In Ref. 20, please mention the location of the publisher.

AU9: Ref. 41 is duplicate of Ref. 9. Hence duplicate entry has been deleted and references have been renumbered. Please check. Correct

EDITOR QUERY FOR SORO-2020-0065-VER9-FANG_1P

EQ1: Please check the article type. Research Paper